ChemComm

RSC Publishing

COMMUNICATION

View Article Online
View Journal | View Issue

Li_4NiTeO_6 as a positive electrode for Li-ion batteries†

Cite this: *Chem. Commun.*, 2013, **49**, 11376

Received 6th September 2013,
Accepted 4th October 2013

DOI: 10.1039/c3cc46842a

www.rsc.org/chemcomm

M. Sathiya,[a] K. Ramesha,[b] G. Rousse,[c] D. Foix,[de] D. Gonbeau,[de] K. Guruprakash,[b] A. S. Prakash,[b] M. L. Doublet[ef] and J.-M. Tarascon*[ae]

Layered Li_4NiTeO_6 was shown to reversibly release/uptake ~2 lithium ions per formula unit with fair capacity retention upon long cycling. The Li electrochemical reactivity mechanism differs from that of Li_2MO_3 and is rooted in the Ni^{4+}/Ni^{2+} redox couple, that takes place at a higher potential than conventional $LiNi_{1-x}Mn_xO_2$ compounds. We explain this in terms of inductive effect due to Te^{6+} ions (or the TeO_6^{6-} moiety).

At their early stages (1991), commercial Li-ion batteries were using two intercalation compounds $LiCoO_2$ and graphite as positive and negative electrodes, respectively.[1] Since then, layered oxides have garnered increasing interest with numerous compositional attempts to alleviate the high cost and toxicity associated with cobalt, while preserving the large energy densities resulting from cobalt's high redox voltage and low molecular weight. Through such an exploration, nickel based compounds such as $LiNi_{0.33}Mn_{0.33}Co_{0.33}O_2$ and $LiNi_{0.5}Mn_{0.5}O_2$ have been identified to be prime alternatives to $LiCoO_2$ in the battery market, owing to the accessibility of two-electron Ni^{4+}/Ni^{2+} redox process that enables capacities of ~200 mA h g^{-1} to be achieved.[2,3] Additional improvements, leading to capacities higher than 220 mA h g^{-1}, have been made *via* the introduction of lithium-rich layered oxides ($Li_{1+x}Ni_yCo_zMn_{1-x-y-z}O_2$), which are basically considered to be composed of two different layered oxides $LiMO_2$ and Li_2MO_3.[4] Nevertheless, a poor understanding of both their Li-insertion mechanism and continuous voltage decay upon cycling has plagued the commercial use of these Li-rich phases. Addressing these issues has drained humongous research efforts worldwide, but no consensus had been reached until our group explained, *via* a simple chemical approach combining XPS and EPR experiments, that: (i) the extra measured capacity within these materials is rooted in cumulative reversible cationic ($M^{n+} \rightarrow M^{(n+1)+}$) and anionic ($O^{2-} \rightarrow O_2^{2-}$) redox processes, and (ii) that the voltage decay upon cycling can be minimized through Sn-substitution for Ru in $Li_2Ru_{1-y}Sn_yO_3$.[5] We explained the overall mechanism in terms of Ru(4d)–O(2p) hybridization, implying the proximity of Ru-4d and O-2p levels within the material band structure.

Because of the rarity and high cost of Ru, one part of this continuing work is the exploration of Ru-free compounds showing *n*d–sp hybridization and belonging to the $Li_4MM'O_6$ family, which contains a huge number of members, as the only restriction requires that the sum of M and M′ formal oxidation states be equal to 8 to ensure electro-neutrality.[6] Based on the fact that most of the studies addressing holes on oxygen deal with Ni-based oxides,[3] we have selected Ni-based $Li_2Ni_{0.5}Te_{0.5}O_3$ (hereafter represented as $Li_4Ni^{2+}Te^{6+}O_6$) with the hope of achieving high capacity through (i) the $2e^-$ redox process associated with Ni^{4+}/Ni^{2+} as observed for the aforementioned layered oxides $LiNi_{0.33}Mn_{0.33}Co_{0.33}O_2$ and $LiNi_{0.5}Mn_{0.5}O_2$,[2,3] and (ii) oxygen redox activity, provided that a high degree of Ni(3d)–O(2p) hybridization can be achieved.

Li_4NiTeO_6 was prepared by a conventional ceramic method from a stoichiometric mixture of Li_2CO_3 (Aldrich), $NiC_4H_6O_4{\cdot}4H_2O$ and TeO_2 (across organics) (2 : 1 : 1) annealed at about 1000 °C for 18 h, followed by heating at 1050 °C for 6 h with intermediate grinding. 10% Li_2CO_3 was added in excess to compensate lithium loss due to high temperature heat treatment. The structure of the compound was analyzed by Rietveld refinement[7] using the Fullprof program[8] against high-resolution synchrotron powder diffraction data, collected on the 11-BM beamline at the Advanced Photon Source (APS, Argonne National Laboratory) with a wavelength of 0.4138 Å.

Bragg peaks unambiguously indicate that the sample crystallizes in the *C*2/*m* space group with cell parameters a = 5.1584(1) Å, b = 8.8806(1) Å, c = 5.1366(1) Å and β = 110.241(1)° (V = 220.777(3) Å^3), *i.e.* a cell similar to the one reported for Li_2MnO_3.[9] Refinements using different distributions of atoms within the layers led to a structure with Li layers alternating with honeycomb Li/Ni/Te layers (Fig. 1). In the latter, Li and Ni are statistically distributed in the same octahedral site (colored in yellow/green), surrounding TeO_6 octahedra (colored in blue). The final refinement which includes a strain analysis is shown in Fig. 1, and the deduced structural parameters are detailed in ESI† (Fig. S1, Tables S1 and S2).

[a] *LRCS, CNRS UMR 7314, UPJV, 80039 Amiens and Collège de France, 75231 Paris, France. E-mail: jean-marie.tarascon@u-picardie.fr*
[b] *CSIR Central Electrochemical Research Institute, Chennai-unit, India*
[c] *IMPMC, CNRS UMR 7590, UPMC Univ Paris 06, Paris, France*
[d] *IPREM/ECP (UMR 5254), University of Pau, 64053 Pau, France*
[e] *RS2E, FR CNRS 3459, France*
[f] *ICG, CNRS UMR5253, Univ Montpellier 2, France*

† Electronic supplementary information (ESI) available: Structural analysis and orbitals diagram. See DOI: 10.1039/c3cc46842a

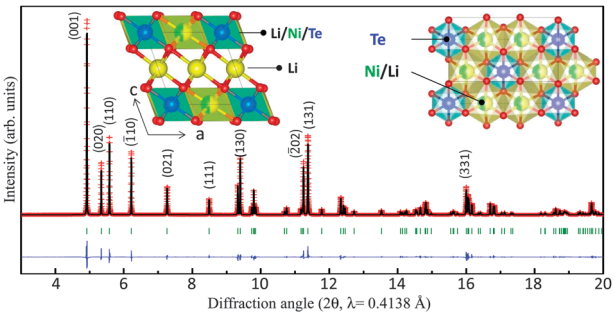

Fig. 1 Structure and Rietveld refinement of Li_4NiTeO_6 (R_{Bragg} = 3.17%, χ^2 = 10.9). Inset: Stacking of Li/Ni/Te layers and Li layers (left), view of one honeycomb Li/Ni/Te layer, for which Li and Ni are equally distributed on the same site (right). Li is yellow, Ni is green, Te is blue and O is red.

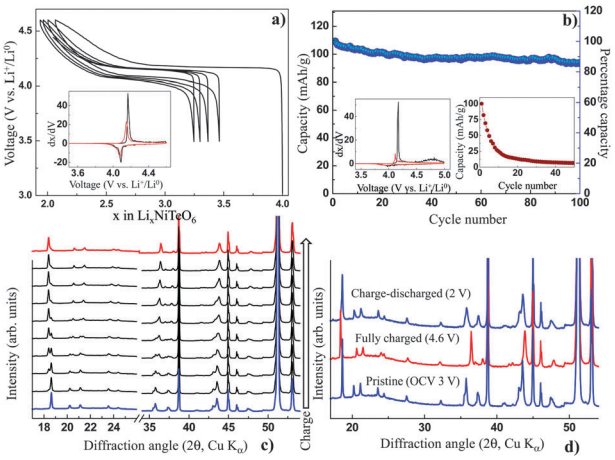

Fig. 2 Electrochemical performance of Li_4NiTeO_6. (a) Voltage *vs.* composition profile for Li_4NiTeO_6, with (as inset) the derivative plot for the first (black) and second (red) cycles. (b) Capacity retention for a Li/Li_4NiTeO_6 cell together with (lower left inset) a derivative plot for the first (black) and second (red) cycles on cycling to a higher voltage (2 to 5 V); (lower right inset) a capacity retention plot when the cell is cycled over 2 to 5 V. (c) *In situ* XRD patterns (λ_{Cu}) while Li_4NiTeO_6 is charged at a C/20 rate, (d) patterns collected for the pristine electrode, charged to 4.6 V and fully discharged issued from (c).

Electrochemical behaviour of Li_4NiTeO_6 as a cathode material has been explored in lithium half cells (Swagelok™ cells) using 1 M $LiPF_6$ in EC : PC : DMC (1 : 1 : 3 wt ratio) as an electrolyte. The working electrode was made by milling the sample with 20% carbon black (Super P, Timcal) using a high energy SPEX 800 miller for 20 minutes. The voltage-composition trace is shown in Fig. 2a. Upon charging, the cell rapidly reaches a voltage plateau located at 4.2 V *vs.* Li^+/Li, which lasts until the removal of ~1.5 Li^+ ions, prior to smoothly and continuously increasing to 4.6 V through the end of charging process which corresponds to total removal of ~2 Li^+ ions solely based on electron counting. The following discharge shows an identical profile (smooth decay + plateau), but is shorter since solely 1.5 Li^+ ions are reinserted upon discharge. Such a large irreversibility between the first charge and discharge is reminiscent of some electrolyte decomposition at high potential, thus leading to uncertainty in the amount of Li reinserted, which is below 2, as we will show later on using XPS. This leads to an overall reversible capacity of 110 mA h g^{-1} for Li_4NiTeO_6 which is sustained upon cycling since the cell retains nearly 90% of its initial capacity after 100 cycles (Fig. 2b). The derivative plot shown in the inset of Fig. 2a confirms a single redox process upon cycling. Increasing the charging potential to 5 V showed a small broad second oxidation peak (left inset in Fig. 2b) centred at 4.8 V and a rapid decay of cell performance upon cycling (right inset in Fig. 2b). Such capacity decay is mainly rooted in a voltage-driven transformation/decomposition of Li_4NiTeO_6, as suggested by high degree of amorphisation of the 5 V oxidized sample.

Overall, the voltage profile of Li/Li_4NiTeO_6 cells drastically differs from those measured previously for Li/$Li_2Ru_{1-y}M_yO_3$ (M = Sn, Mn)[5,10] cells, as they present a single voltage plateau upon consecutive cycles instead of a stair-case charge profile followed by a S-type curve upon discharge. This indicates a different lithiation–delithiation mechanism that we have explored by both *in situ* XRD and XPS measurements.

Fig. 2c shows the XRD patterns collected during the charge of a home-made Li/Li_4NiTeO_6 electrochemical cell equipped with a Be window. Upon removal of Li, there is appearance of a set of weak Bragg peaks which grow at the expense of the peaks of the pristine phase, and become single phase after the removal of 2 lithium ions. This new $Li_{4-x}NiTeO_6$ phase, formed at the end of charge (4.6 V), with x being not accurately defined due to competing electrolyte oxidation, can also be indexed to a *C*2/*m* monoclinic cell with lattice parameters a = 5.037(1) Å, b = 8.716(1) Å, c = 5.163(1) Å; β = 108.79(1)°, *i.e.* a volume of 214.61(5) Å^3 which is less than 3% smaller than that of pristine phase. The *c*-lattice parameter increase upon Li removal arises from increasing repulsion between MO_2 layers which become less screened by Li-ions, while the decrease in both a and b lattice parameters originates from the cation size reduction linked to the $Ni^{2+} \rightarrow Ni^{4+}$ oxidation process. Upon discharge, the XRD pattern for the fully discharged material being similar to that of the pristine phase (Fig. 2d) indicates the structural reversibility of the electrochemical process. A closer examination of the lattice parameter values indicated a slightly lower unit cell volume for the charged–discharged sample (V = 219.28 Å^3 *vs.* 220.78 Å^3), suggesting the presence of tiny amounts of smaller Ni^{4+} (lower ionic radii than Ni^{2+}) in the reduced sample as confirmed by XPS.

XPS analyses (Fig. 3) were carried out for pristine Li_4NiTeO_6 electrode mixed with 20% carbon (a), and similar electrodes charged to 4.6 V (b), and charged to 4.6 V and then discharged to 2 V (c). The Ni-2$p_{3/2}$ core spectra for the pristine sample show a main peak at 855.6 eV and a satellite peak at 861.7 eV, confirming the presence of Ni^{2+} in the pristine phase.[11] Upon charging to 4.6 V, the Ni-2$p_{3/2}$ peak shifts to a higher binding energy (856.7 eV) which corresponds to Ni^{4+} with a small shoulder indicative of remaining part of Ni^{2+} which we could estimate to be ~20% by XPS analysis. This agrees with our electrochemical measurements, indicating minor electrolyte decomposition so that all charging current is not fully used to oxidize Ni^{2+} to Ni^{4+}. Upon discharge, the Ni-2$p_{3/2}$ binding energy shifts back to that of pristine phase, confirming mainly the reversibility of the process with a very small amount of residual Ni^{4+} (tiny shoulder in the left of the Ni^{2+} peak) in agreement with the electrochemical data. Turning to Te-3d core spectra, the Te-3$d_{5/2}$ peak at 576.3 eV is characteristic of Te^{6+} referenced to Li_4TeO_5 and Li_2TeO_3 (Te-3$d_{5/2}$ respectively at 576.3 eV and 575.9 eV). It remains unaltered for the entire charge–discharge process indicating that Te does not participate

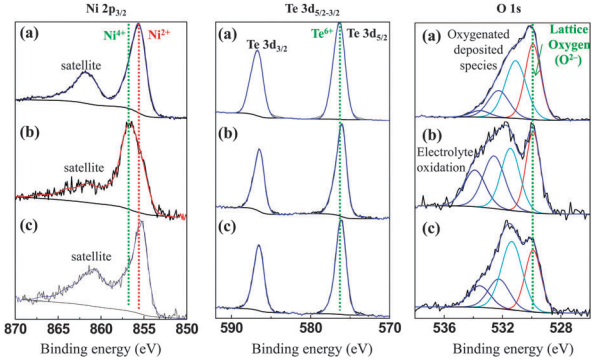

Fig. 3 XPS spectra of Ni-2p, Te-3d and O1s core peaks of (a) the Li_4NiTeO_6 pristine electrode, (b) charged to 4.6 V, (c) further discharged to 2.0 V.

in the redox process.[12] Lastly, the O-1s core spectra of the aforementioned samples were collected to check for eventual observation of peroxo-like species as seen with $Li_2Ru_{1-y}M_yO_3$ compounds reported earlier.[5,10] The peaks characteristic of O^{2-} anions belonging to the crystalline network at 529.9 eV and weakly adsorbed surface species are visible in the pristine sample spectra. The O-1s spectra of the charged sample show an increase of the high binding energy components ($\sim$532.5 eV and $\sim$534.0 eV) ascribed to some oxidation of the electrolyte,[13] however no significant change in the O-lattice/(Ni + Te) atomic ratio was observed between the pristine and charged samples, in line with the absence of an additional peak which could be due to formation of peroxo-like species. However, caution should be exercised here, owing to the broadness of the collected spectra for the charged samples.

Conclusively, the electrochemical behaviour of Li_4NiTeO_6 differs from other reported Li-rich layered oxides and Mn/Sn-substituted Li_2RuO_3 systems, although they all belong to the same structural family. The main difference lies in the shape of cycling profile, which shows a classical two-phase insertion–deinsertion process. This indirectly implies the non-participation of anionic species in contrast to $Li_2Ru_{1-y}M_yO_3$ (M = Mn, Sn) system, suggesting that the total capacity of Li_4NiTeO_6 can simply be explained on the basis of a classical insertion process involving the Ni^{4+}/Ni^{2+} redox couple. This is further confirmed by full preservation of the host framework throughout cycling as deduced by XRD.

Overall, the insertion mechanism in Li_4NiTeO_6 can be compared with typical intercalation seen in layered $LiNi_{0.5}Mn_{0.5}O_2$ and not with that of $Li_2Ru_{1-y}M_yO_3$ (M = Mn, Sn), the reason most likely being that the 3d energy levels associated with Ni^{2+} are higher in energy than the 4d levels of Ru^{4+}, therefore diminishing the chances of undergoing pronounced M(*n*d)–X(*n*p) metal–ligand hybridization. The absence of two distinct steps corresponding to the Ni^{2+}/Ni^{3+} and Ni^{3+}/Ni^{4+} redox processes as Ni^{2+} is oxidized to Ni^{4+} is most likely due, as explained for $LiNi_{0.5}Mn_{0.5}O_2$, to the overlapping of two redox couples.[3]

Lastly, the higher Ni^{2+}/Ni^{4+} redox voltage observed for Li_4NiTeO_6 (4.2 V) as compared to other Ni^{2+}-based layered oxides ($<$4 V) can simply be explained by considering Te^{6+} in Li_4NiTeO_6 as a TeO_6^{6-} moiety. This TeO_6^{6-} anion – being more electronegative than O^{2-} – increases the redox potential through its inductive effect, as observed in polyanionic compounds when SO_4^{2-} units are replaced by PO_4^{3-} for instance. The significant increase in potential through this inductive effect is related to the closeness in energy of the Te(5p) orbitals and O(2p) orbitals, as depicted in Fig. S2, ESI.† Specifically, the strong Te(5p)–O(2p) hybridization lowers the electron density on the Ni–O bonds, consequently increasing their ionic character and therefore the energy required to oxidise Ni^{2+} to Ni^{4+}. This is confirmed by XPS as the (O-1s lattice – Ni-2p$_{3/2}$) binding energy difference of 326.7 eV is higher (by 0.3 – 0.4 eV) than values reported for Ni^{2+} based layered oxides.[11,14] This chemical approach combined with simple concepts of orbital interactions could provide an interesting means for tuning the potential of Ni^{4+}/Ni^{2+} redox couple in other layered oxides. A variety of other Li_4NiMO_6 compounds are being presently tested to fully validate this point.

To summarize, we have reported that the layered oxide Li_4NiTeO_6 reversibly reacts with 1.5 Li^+ at a potential of 4.2 V *vs.* Li^+/Li^0 through a classical insertion mechanism involving the Ni^{4+}/Ni^{2+} redox couple. With a capacity of only 110 mA h g^{-1} and the use of a toxic element such as Te, the practical interest in this phase is limited clearly. Still, this could be made useful for practical applications provided a less heavy and toxic initiator can be found to replace Te^{6+}. From a fundamental standpoint, however, this study stresses that the design of compounds showing both anionic and cationic redox activities is not trivial in the absence of theoretical support. Ni was obviously not the right choice, presumably due to large separation between Ni^{4+}-3d levels and O-2p levels. This is an open call to theorists for evaluating the M(*n*d)–X(*n*′p) metal–ligand hybridization strength in these layered $Li_4MM'O_6$ oxides for various M and M′, and additionally for testing our findings about the feasibility of tuning the redox voltage of M *via* the proper choice of an inactive M′ cation. We await fruitful experimentalist–theorist interactions.

Use of the APS at ANL supported by the U.S. Department of Energy under Contract No. DE-AC02-06CH11357 is greatly acknowledged.

Notes and references

1 T. Nagaura and K. Tozawa, *Prog. Batteries Sol. Cells*, 1990, **9**, 209.
2 T. Ohzuku and Y. Makimura, *Chem. Lett.*, 2001, 642.
3 S. B. Schougaard, J. Breger, M. Jiang, C. P. Grey and J. B. Goodenough, *Adv. Mater*, 2006, **18**, 905.
4 M. M. Thackeray, S.-H. Kang, C. S. Johnson, J. T. Vaughey, R. Benedek and S. A. Hackney, *J. Mater. Chem*, 2007, **17**, 3112.
5 M. Sathiya, G. Rousse, K. Ramesha, C. P. Laisa, H. Vezin, M. T. Sougrati, M.-L. Doublet, D. Foix, D. Gonbeau, W. Walker, A. S. Prakash, M. Ben Hassine, L. Dupont and J.-M. Tarascon, *Nat. Mater.*, 2013, **12**, 827.
6 V. Kumar, N. Bhardwaj, N. Tomar, V. Thakral and S. Uma, *Inorg. Chem.*, 2012, **51**, 10471.
7 H. M. Rietveld, *J. Appl. Crystallogr.*, 1969, **2**, 65.
8 J. Rodríguez-Carvajal, *Physica B*, 1993, **192**(1–2), 55.
9 P. Strobel and B. L. Andron, *J. Solid State Chem.*, 1988, **75**(1), 90.
10 M. Sathiya, K. Ramesha, G. Rousse, D. Foix, D. Gonbeau, A. S. Prakash, M.-L. Doublet, K. Hemalatha and J.-M. Tarascon, *Chem. Mater.*, 2013, **25**(7), 1121.
11 N. Yabuuchi, Y.-C. Lu, A. N. Mansour, T. Kawaguchi and Y. Shao-Horn, *Electrochem. Solid-State Lett.*, 2010, **13**(11), A158.
12 A. Gupta, C. B. Mullins and J. B. Goodenough, *J. Power Sources*, 2013, **243**, 817.
13 R. Dedryvère, D. Foix, S. Franger, S. Patoux, L. Daniel and D. Gonbeau, *J. Phys. Chem. C*, 2010, **114**, 10999.
14 Q. Jiang, K. Du and Y. He, *Electrochim. Acta*, 2013, **107**, 133.

